Atmosphere **2014**, *5*, 557-574; doi:10.3390/atmos5030557

OPEN ACCESS

atmosphere

ISSN 2073-4433

www.mdpi.com/journal/atmosphere

Article

Airborne Vertical Profiling of Mercury Speciation near Tullahoma, TN, USA

Steve Brooks [1,2], Xinrong Ren [1,3,4,*], Mark Cohen [1], Winston T. Luke [1], Paul Kelley [1,3], Richard Artz [1], Anthony Hynes [5], William Landing [4] and Borja Martos [2]

[1] Air Resources Laboratory, National Oceanic and Atmospheric Administration, 5830 University Research Court, College Park, MD 20740, USA; E-Mails: sbrooks@utsi.edu (S.B.); Mark.Cohen@noaa.gov (M.C.); Winston.Luke@noaa.gov (W.T.L.); Paul.Kelley@noaa.gov (P.K.); Richard.Artz@noaa.gov (R.A.)

[2] Department of Mechanical, Aerospace and Biomedical Engineering, University of Tennessee Space Institute, 411 BH Goethert Parkway, Tullahoma, TN 37388, USA; E-Mail: bmartos@utsi.edu

[3] Cooperative Institute for Climate and Satellites, University of Maryland, 5825 University Research Court, College Park, MD 20740, USA

[4] Department of Earth, Ocean, and Atmospheric Science, Florida State University, 117 North Woodward Avenue, Tallahassee, FL 32306, USA; E-Mail: wlanding@fsu.edu

[5] Rosenstiel School of Marine and Atmospheric Science, University of Miami, 4600 Rickenbacker Causeway, Miami, FL 33149, USA; E-Mail: ahynes@rsmas.miami.edu

* Author to whom correspondence should be addressed; E-Mail: Xinrong.Ren@noaa.gov; Tel.: +1-301-683-1391; Fax: +1-301-683-1370.

Received: 12 April 2014; in revised form: 19 July 2014 / Accepted: 25 July 2014 / Published: 13 August 2014

Abstract: Atmospheric transport and *in situ* oxidation are important factors influencing mercury concentrations at the surface and wet and dry deposition rates. Contributions of both natural and anthropogenic processes can significantly impact burdens of mercury on local, regional and global scales. To address these key issues in atmospheric mercury research, airborne measurements of mercury speciation and ancillary parameters were conducted over a region near Tullahoma, Tennessee, USA, from August 2012 to June 2013. Here, for the first time, we present vertical profiles of Hg speciation from aircraft for an annual cycle over the same location. These airborne measurements included gaseous elemental mercury (GEM), gaseous oxidized mercury (GOM) and particulate bound mercury (PBM), as well as ozone (O_3), sulfur dioxide (SO_2), condensation nuclei (CN) and meteorological parameters. The flights, each lasting ~3 h, were conducted typically one

week out of each month to characterize seasonality in mercury concentrations. Data obtained from 0 to 6 km altitudes show that GEM exhibited a relatively constant vertical profile for all seasons with an average concentration of 1.38 ± 0.17 ng·m^{-3}. A pronounced seasonality of GOM was observed, with the highest GOM concentrations up to 120 pg·m^{-3} in the summer flights and lowest (0–20 pg·m^{-3}) in the winter flights. Vertical profiles of GOM show the maximum levels at altitudes between 2 and 4 km. Limited PBM measurements exhibit similar levels to GOM at all altitudes. HYSPLIT back trajectories showed that the trajectories for elevated GOM (>70 pg·m^{-3}) or PBM concentrations (>30 pg·m^{-3}) were largely associated with air masses coming from west/northwest, while events with low GOM (<20 pg·m^{-3}) or PBM concentrations (<5 pg·m^{-3}) were generally associated with winds from a wider range of wind directions. This is the first set of speciated mercury vertical profiles collected in a single location over the course of a year. Even though there are current concerns that the KCl denuders used in this study may under-collect GOM, especially in the presence of elevated ozone, the collected data in this region shows the strong seasonality of oxidized mercury concentrations throughout the low to middle free troposphere.

Keywords: atmospheric mercury; gaseous elemental mercury; gaseous oxidized mercury; particulate-bound mercury; airborne measurements; vertical profile; HYSPLIT

1. Introduction

Airborne measurements of mercury speciation in the free troposphere are rare due to the expense of aircraft operation, the sensitive nature of the sampling and the need to pre-concentrate the mercury species. Swartzendruber *et al.* [1] conducted five summertime flights over Washington State and measured the vertical distributions of gaseous elemental mercury (GEM) and gaseous oxidized mercury (GOM). GOM concentrations were determined both by using the difference between total gaseous Hg (TGM) and GEM and by GOM collection onto KCl coated quartz denuders. For both techniques, the GOM concentration was lowest close to the surface (<1 km) and had a broad peak between 2 and 4 km altitude. The two techniques for measuring GOM concentrations were well correlated, but there was a nearly consistent factor of two difference in concentrations, with KCl denuders showing lower GOM concentrations. Over the five flights, the maximum GOM concentrations at 2–4 km altitude were ~150 and 75 pg·m^{-3} for the difference and denuder methods, respectively.

Murphy *et al.* [2] and, most recently, Lyman and Jaffe [3] conducted aircraft campaigns showing that Hg in the tropopause and lower stratosphere is predominately in an oxidized form. Lyman and Jaffe [3] reported GEM depletions near the tropopause and lower stratosphere, suggested *in situ* oxidation of GEM to GOM and particulate bound mercury (PBM) and reported that subsidence was likely a significant source of oxidized mercury in the free troposphere.

Long-term ground-based measurements near mountain peaks suggest that under certain conditions sampling of free tropospheric air is possible. Fain *et al.* [4] at Storm Peak Laboratory, Colorado, observed episodic elevated GOM concentrations to levels of 137 pg·m^{-3}. These events were attributed to deep vertical mixing to the ground level of middle tropospheric air enriched in GOM [4]. Similarly,

Swartzendruber *et al.* [5] at Mt. Bachelor Observatory, Oregon, attributed observed nighttime decreases in GEM concentration and enhancements in GOM concentration to air transported from the free troposphere during nocturnal down slope winds. Most recently, at the Mauna Loa Observatory, Hawaii, enhancements of GOM up to ~400 pg·m^{-3} have been observed and attributed to transport from the free troposphere [6].

Vertical modeling of GEM and GOM in the troposphere over North America was summarized by Bullock *et al.* [7]. The various models included were the Atmospheric and Environmental Research (AER), Inc., Global Chemical Transport Model for Mercury (CTM-Hg) [8], the Goddard Earth Observing System (GEOS-Chem) model [9] and the global/regional atmospheric heavy metals model (GRAHM) [10]. Over our study area in Tennessee, the three models predict low GOM concentrations (<20 pg·m^{-3}) in the near-surface air with enhancements beginning above the boundary layer with concentrations in the range of ~30 to 120 pg·m^{-3} at an altitude of 3 km [7]. Other modeling by Holmes *et al.* [11] suggests that 47% of GEM tropospheric oxidation takes place above 5.5 km, 32% in the middle troposphere between 2.1 and 5.5 km and 21% below 2.1 km.

In this paper, we present, for the first time, monthly vertical profiles of Hg speciation and ancillary measurements from aircraft for an annual cycle over the same location. This study was conducted to examine potential transport from the upper troposphere to the lower troposphere and potential correlations of Hg species aloft to Hg concentrations at the surface. Additional goals were to provide data to evaluate and improve models, identify potential oxidation pathways and assess the relative contributions of natural and anthropogenic processes to local, regional and global Hg burdens.

2. Results and Discussion

2.1. A Typical Flight

Daily flights, with the exception of a single nighttime flight, departed at a local time of 10:00 (am) ± 45 min. During a typical 3-h flight, GEM, ozone, SO_2, condensation nuclei (CN) and meteorological parameters were measured continuously, while the GOM and PBM samples were collected for 30-min periods in altitude "blocks" during ascent and descent, as shown in Figure 1. During the flight, the average ground speed was ~69 ± 10 m·s^{-1}, so the distance the airplane traveled during the 30 min period was on the order of 120 km.

Typical sampling data, including GEM, GOM, PBM, O_3, SO_2, CN, temperature, pressure, dew point and solar radiation from a single flight on 23 November 2012, are shown in Figure 2. GOM and PBM were collected in 30-min samples on the ascent and descent. In an unpressurized aircraft, the normal rate of ascent and descent is about 150 m·min^{-1}; thus requiring ~40 min to climb or descend ~6 km. Given the high hourly cost of aircraft, we made use of the ascent and descent times in our sampling.

2.2. Overall Hg Speciation

An overall statistical summary of the airborne and ground-based mercury measurements during this study is shown in Table 1. Average concentrations were 1.38 ± 0.17 ng·m^{-3} for GEM, 34.3 ± 28.9 pg·m^{-3} for GOM and 29.6 ± 29.5 pg·m^{-3} for PBM. Maximum concentrations were 2.05 ng·m^{-3} for GEM, 125.6 pg·m^{-3} for GOM and 194.9 pg·m^{-3} for PBM.

Figure 1. Time series of flight altitude during a typical flight on 13 November 2012. Denuder and regenerable particulate filter (RPF) samples were collected while the airplane was ascending or descending with 30-min sampling intervals for each denuder/RPF set. Samples were usually collected above the boundary layer.

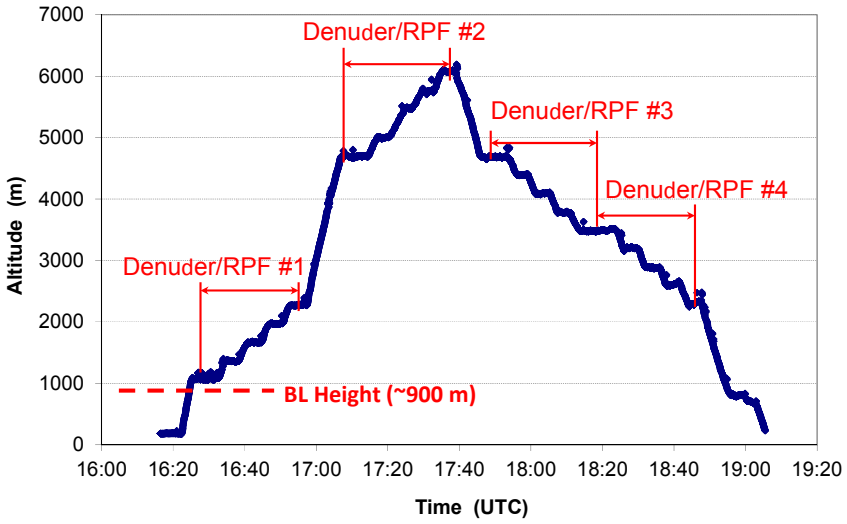

Figure 2. Time series of altitude, gaseous elemental mercury (GEM), gaseous oxidized mercury (GOM), particulate bound mercury (PBM), O_3, and SO_2 (**Left**), as well as condensation nuclei (CN), temperature, pressure, dew point and photosynthetically active radiation (PAR) (**Right**) during the flight on 13 November 2012.

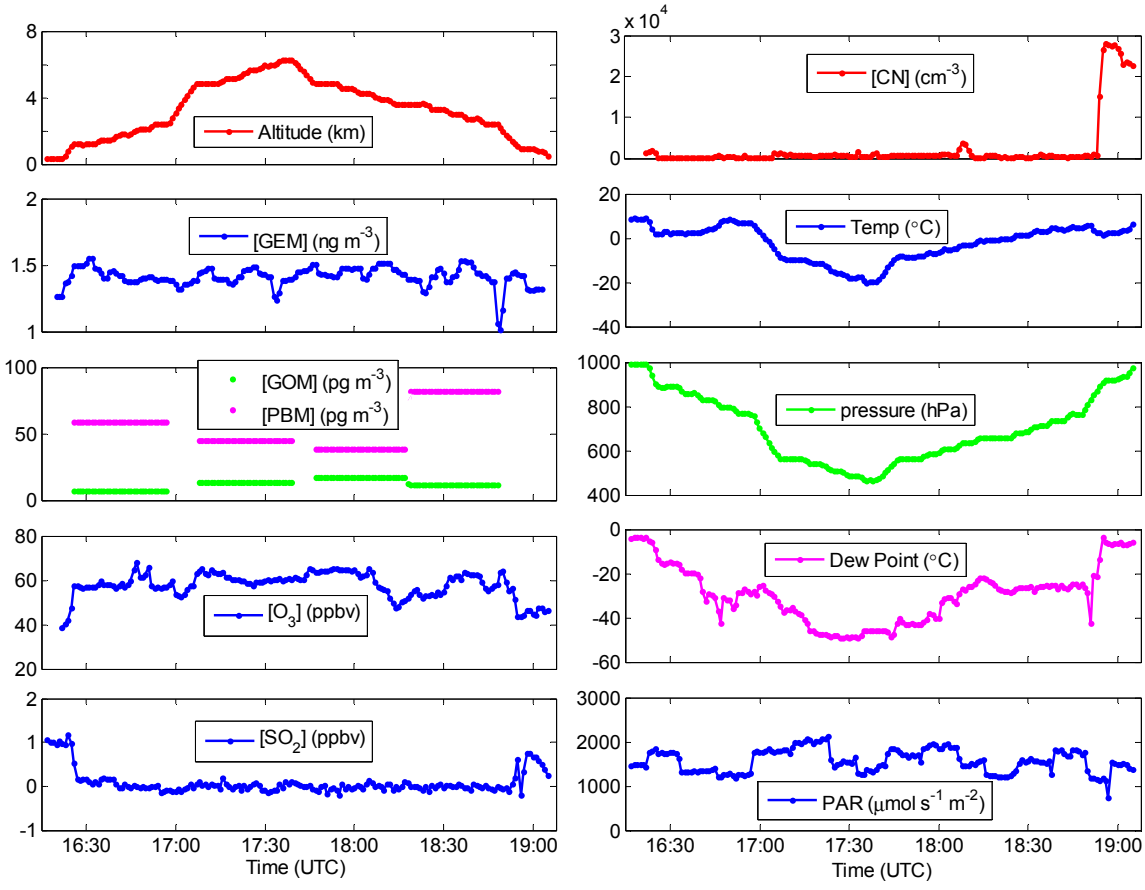

Table 1. Statistical summary of airborne and ground measurements of mercury species.

Species	Sample #	Max (pg·m^{-3})	Min (pg·m^{-3})	Mean ± SD (pg·m^{-3})	Median (pg·m^{-3})
GEM_air *	1813	2050	750	1380 ± 174	1400
GOM_air *	106	125.6	3.1	34.3 ± 28.9	22.5
PBM_air *	53	194.9	4.4	29.6 ± 29.5	25.3
GEM_gnd **	26	1610	1170	1350 ± 109	1320
GOM_gnd **	27	12.3	0.6	2.3±2.4	1.80

* Airborne measurements; ** ground measurements.

2.2.1. GEM

The GEM vertical profile for each month showed relatively uniform vertical profiles from August 2012 to February 2013, from the surface to 6 km (Figure 3). Three individual GEM profiles for April, May and June 2013, represented just a single flight per month and showed decreasing GEM above the boundary layer (>1.5 km). However, the GEM range of these three flights was within the variation of some individual flights during other months, and therefore, the GEM difference of these three months from other months could be due to normal day-to-day variation (Figure 3). Also of note is the substantial GEM enhancement above 4 km for two flights in September 2012, which was coincident with enhanced condensation nuclei (CN). This might be due to regional or long-range transport of air pollution rich in both CN and GEM at this altitude. More measurements and modeling work would be needed in order to confirm this speculation.

Figure 3. Vertical profile of GEM concentrations: all data points with 2.5 min intervals (**Left**) and mean vertical profile for each month of flights (**Right**). The black line represents mean GEM levels in 0.5-km altitude bins.

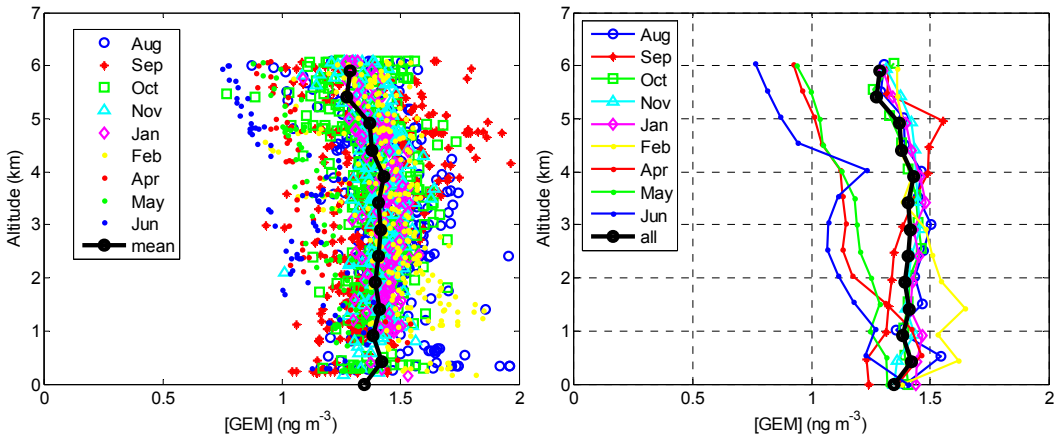

2.2.2. GOM

In contrast to GEM, vertical profiles of GOM show large variations (Figure 4). Each KCl denuder collected GOM over a block of altitude over a 30-min time period. With the exception of January 2013, which showed little vertical variation, GOM concentration maxima were consistently measured between 2 and 4.5 km (Figure 5).

Figure 4. Vertical profile of GOM concentrations. All GOM measurements had a duration of 30 min. Each symbol line represents the GOM concentration of a 30-min sample over the corresponding altitude range. The linked black circles represent the mean vertical profile for all measurements.

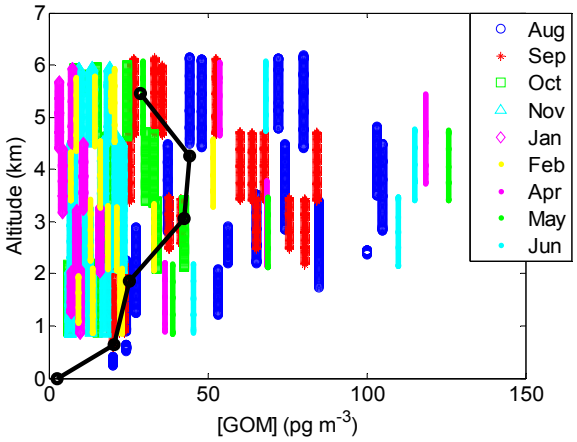

Figure 5. (**Left**) Mean vertical profile of GOM for each month of flights from August 2012 to January 2013 (**Right**) mean vertical profile of GOM for each month of flights from January 2013 to June 2013.

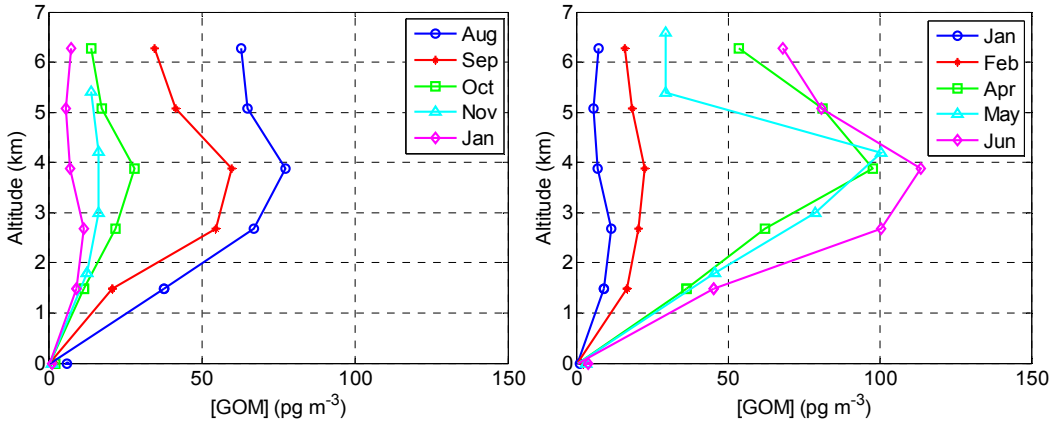

GOM showed a strong seasonal variation. Overall, GOM levels continuously dropped from August to January, were minimum in January and increased from February to June (Figure 5). We observed that GOM concentration at an altitude of ~2–4 km was 10–30-times higher than GOM concentrations in the near-surface air (shown at an altitude of 0 km in Figure 5) and that the ground measurements of GOM did not correlate with the GOM above the boundary layer (r^2 = 0.13; detailed sample data not shown). The airborne GOM concentration showed a strong seasonality with "winter" minima in November to February (we did not conduct measurements in December) and "summer" maxima in April to August (we did not conduct measurements in July and only one flight was performed each month in April, May and June 2013). The spring/summer maximum observed in this study is consistent with other measurements made in the southeastern United States (e.g., [12]). GOM during the "summer" (April to August) showed lower concentrations below ~2 km, which is often the summertime midday boundary layer height.

2.2.3. PBM

Measurements of PBM began in October 2012, two months after the study started. Similar to GOM, each University Research Glassware (URG) filter tube downstream of a KCl denuder collected PBM over a block of altitude over a 30-min time period. The URG filter tube we used was essentially the same as the regenerable particulate filter (RPF) used in the commercial Tekran 1135 instrument. The slight difference of our filter tube was in the inlet/outlet connectors in order to fit the aircraft configuration. No PBM measurements were conducted at the ground level, due to resource constraints. As shown in Figure 6, PBM showed "winter" minima in January and February and "summer" maxima in June through October. Little vertical variations were noted in the winter months; however, during summer months, a significant peak occurred in the range of 3–4.5 km with lower PBM at higher altitudes.

Figure 6. Vertical profile of PBM concentrations. (**Left**) All PBM measurements with 30-min intervals. Each symbol line represents the PBM concentration of a 30-min sample over the corresponding altitude range. The linked black diamonds represent the mean vertical profile of all measurements; (**Right**) the mean vertical profile for each month of flights from October 2012 to June 2013.

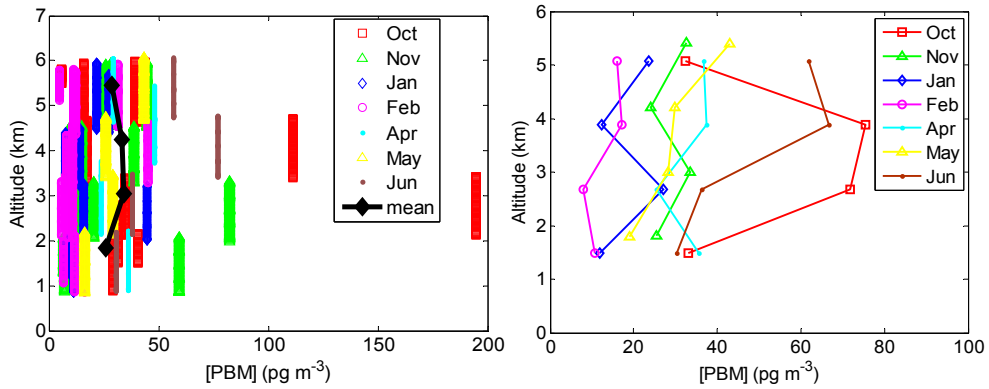

Surprisingly, our results from a single nighttime flight (11 pm–2 am local time) on 18 October 2012, did not differ significantly from our mid-day measurements earlier that same day. Due to logistical difficulties and the lack of differences in Hg concentrations between the midday and midnight flights on 18 October 2012, we did not conduct any additional nighttime flights.

2.3. Other Supporting Measurements

Figure 7 shows vertical profiles of the ancillary measurements of ozone (O_3), sulfur dioxide (SO_2) and condensation nuclei (CN). O_3 concentrations were relatively low in the boundary layer and relatively constant in the free troposphere. In general, ozone was elevated during the summer months with peak values in August and September, as would be expected. SO_2 was occasionally elevated in the boundary layer, but was near-zero above the boundary layer. Condensation nuclei were generally low with episodic peaks within the boundary layer and at 5–6 km. Overall, the vertical profiles of GEM and GOM were not significantly correlated with ozone (r^2 = 0.01 and sample number N = 4,371 for GEM and r^2 = 0.06 and N = 107 for GOM), sulfur dioxide (r^2 = 0.002 and N = 3,042 for GEM and r^2 = 0.006

and N = 107 for GOM) or condensation nuclei (r^2 = 0.002 and N = 3,874 for GEM and r^2 = 0.02 and N = 107 for GOM) with all *p*-values greater than 0.1.

Figure 7. Vertical profiles of ancillary measurements of ozone (**a**), sulfur dioxide (**b**), and condensation nuclei (**c**) for the entire study. Individual symbols represent 1-min data points, and the linked black circles are averages in 0.5-km altitude bins.

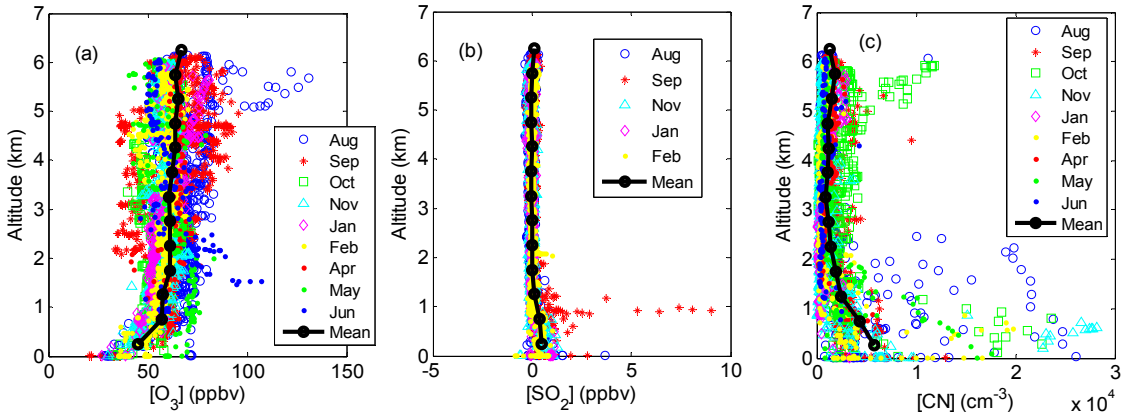

2.4. Oxidation of GEM via Hydroxyl Radical

Major uncertainties in current atmospheric mercury models arise from calculated GEM oxidation rates via ozone, hydroxyl radical (OH) and Br [13]. The hydroxyl radical (OH) is a major oxidizing agent in the troposphere and, with ozone, was the first oxidizer postulated for GEM in the troposphere [14]. Model estimates of the GEM lifetime with respect to OH oxidation [15,16] were approximately 120 days in the troposphere. The OH oxidation mechanism then fell out of favor when [17] and [18,19] concluded that the product of GEM + OH → Hg(OH) was too shorted-lived to be atmospherically relevant. Calvert and Lindberg [20] further suggested that OH oxidation of GEM might be too slow to account for the observed atmospheric lifetime of GEM. A review by Hynes *et al.* [21] determined that the OH initiated oxidation of GEM was unlikely, but that more direct observations of HgOH lifetime and reactivity were needed to resolve its potential atmospheric importance. In spite of these arguments against OH, current atmospheric Hg models (e.g., [22,23]) include ozone, OH and Br as oxidizing agents. Holmes *et al.* [13] concluded that Br is likely more influential over the ocean and the polar regions, but that OH and/or ozone may be more significant over regions, such as the southeastern continental USA where Br levels are low.

To a first approximation, OH can be considered to be a product of sunlight, ozone and water vapor. The primary tropospheric production of OH at temperate latitudes is:

$$O_3 + h\nu \rightarrow O_2 + O(^1D) \quad (1)$$

$$O(^1D) + H_2O_{(g)} \rightarrow 2\ OH \quad (2)$$

In the first reaction, the formed $O(^1D)$ can be quenched by collisions with molecular oxygen and nitrogen to the lower-energy $O(^3P)$ state while a smaller fraction (1%–20%) reacts with water vapor, producing OH via the second reaction. The primary loss mechanisms for OH at temperate latitudes are

the oxidation of CO and CH_4, giving OH a tropospheric lifetime of 0.1 to 1.0 s. With this short of a lifetime, OH concentrations are determined by local chemical processes rather than transport [24,25].

Approximate, modeled OH profiles are shown in Figure 8, adapted from Fishman and Crutzen [24], for average [OH] concentrations at solar-noon for our study location on January 1, April 1, July 1 and October 1. The Fishman and Crutzen [24] model is a quasi-steady state photochemical numerical simulation developed to calculate the tropospheric distribution of OH. The OH concentrations are highest in the summer (July) and lowest in the winter (January). The modeled OH vertical gradient over our profile altitudes (0–6 km) was minimal in winter (January) and maximum (decreasing with height) in summer (July), roughly consistent with our observed gradients of GOM and PBM in winter and above 4 km in summer. We speculate that below ~3 km, removal processes, related to deep summertime boundary layer entrainment, downward mixing and surface sinks, deplete GOM and PBM at a rate exceeding their production via oxidation. In additional to the seasonality of GOM concentration, its monthly profile averages were strongly correlated (r^2 = 0.83; maximum OH *versus* averaged GOM concentration to our modeled hydroxyl radical concentrations, as were maximum OH *versus* average PBM (r^2 = 0.67). In addition, for the months when both GOM and PBM were measured, the total oxidized mercury (averaged monthly peak GOM + PBM) and maximum OH showed a correlation of r^2 = 0.94 (Figure 8). The summertime decrease of GOM concentrations at altitudes below ~3 km could be due to entrainment into the atmospheric boundary layer followed by relatively rapid dry or wet deposition.

Figure 8. (**Left**) Modeled OH at solar noon over the study location 1 January, 1 April, 1 July and 1 October (adapted from Fishman and Crutzen [24]); (**Right**) peak GOM + PBM from the monthly mean profiles from the months when both were collected *versus* the monthly modeled OH maxima.

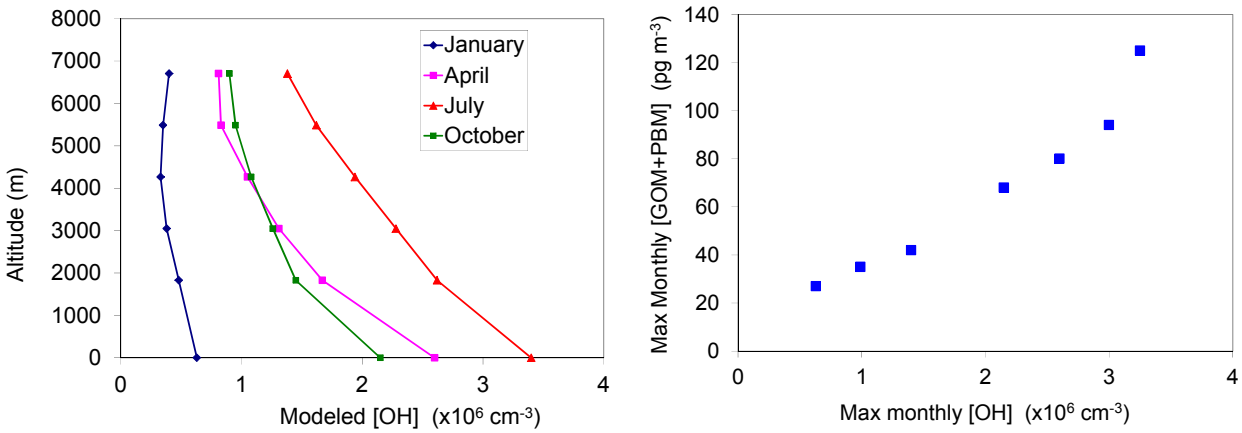

The significant correlation between maximum monthly GOM + PBM and our modeled maximum monthly OH (Figure 8) certainly does not prove that OH plays a major role in GEM oxidation, as correlation does not prove causation. As noted above, Hynes *et al.* [21] and others have argued against OH being a significant oxidizer of GEM. Other explanations might include cloud processes, typically at the top of the summertime boundary layer (~1–1.5 km), or GEM oxidation by halogens, none of which were measured or modeled in this study.

2.5. HYSPLIT back Trajectory Analysis

Two examples of back trajectories for GOM concentration >70 pg·m^{-3} and PBM concentration >30 pg·m^{-3} are shown in the left and middle panels of Figure 9, respectively. We found that back trajectories for GOM concentration >70 pg·m^{-3} or PBM concentration >30 pg·m^{-3} were largely associated with air masses coming from west/northwest, while samples with lower GOM and PBM were generally associated with winds from a wider range of directions. It can also be seen in Figure 9 that the trajectories for different starting altitudes are relative flat, suggesting that there was little downward or upward vertical mixing during those period with enhanced GOM and PBM concentrations. A detailed source-receptor analysis is beyond the scope of this paper. Additional back-trajectory and/or forward dispersion modeling will be necessary to determine the extent to which local/regional sources may have contributed to the levels of mercury seen.

Figure 9. HYSPLIT two-day back trajectories during the flight hours with a starting location of Tullahoma, TN, and starting altitudes at the mid-point of each altitude blocks where airborne GOM and PBM samples were collected. (**Left**) Back trajectories for samples with measured GOM concentration >70 pg·m^{-3}; (**Middle**) back trajectories for samples with measured PBM concentration >30 pg·m^{-3}; (**Right**) back trajectories for all GOM/PBM samples. Blue circles show the locations of large mercury point source emissions in the region, based on the U.S. EPA's 2011 National Emission Inventory. The size of each circle is proportional to the emission rate. The black square at the end of trajectories in each plot represents the flight area.

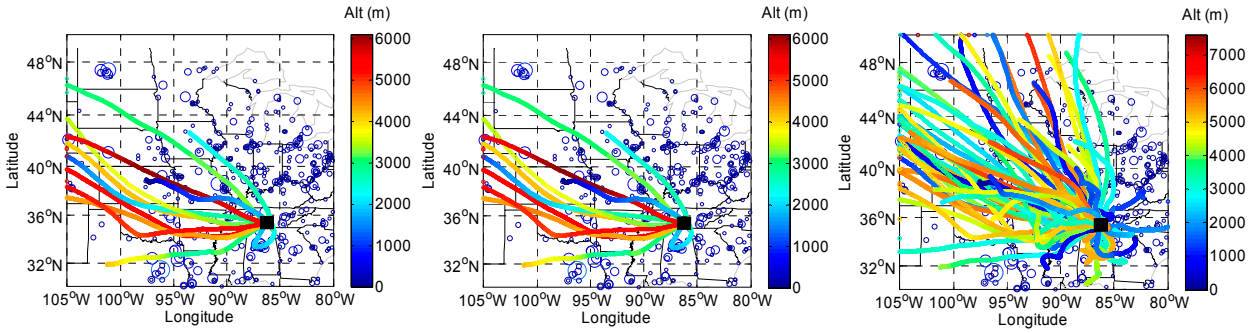

3. Experimental Section

3.1. Study Area

The study was conducted over an area near Tullahoma (35°23′N, 86°14′W), TN, USA, which is located about 110 km southeast of Nashville, TN, USA. To simplify the flight track and to easily accommodate the air traffic control in this region, we requested a square flight area centered on Tullahoma with a length of ~50 km for each side. The U.S. Environmental Protection Agency (EPA) 2011 National Emission Inventory (NEI) shows that there are no significant anthropogenic mercury emission sources within the flight area (within ~100 km) (Figure 10). However, regionally, there are many Hg point sources, mainly power plants and industrial facilities.

Figure 10. Regional anthropogenic mercury point emissions near Tullahoma, TN, USA, as indicated by the open circles with total mercury emission rates greater than 10 kg Hg·yr^{-1}, based on the U.S. EPA's 2011 National Emissions Inventory (NEI). The size of each circle is proportional to the emission amount. The red square in the middle indicates the flight region.

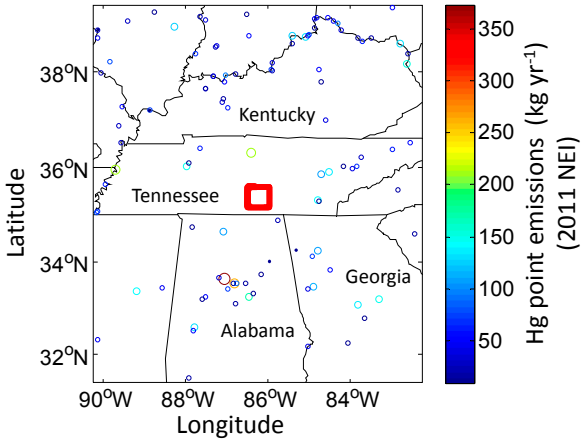

3.2. Measurements

3.2.1. Aircraft Measurements

The University of Tennessee Space Institute (UTSI) Piper Navajo airborne science research aircraft (N11UT) was used in this study to conduct airborne vertical profiling of speciated mercury and other pollutants at altitudes up to ~6 km above ground level in the Tullahoma region. The aircraft was based at Tullahoma Regional Airport (35°23′N, 86°14′W). Airborne measurements of GEM, GOM, PBM, ozone (O_3), sulfur dioxide (SO_2), condensation nuclei (CN) and meteorological parameters (temperature, pressure, dew point and solar radiation) were made (Figure 11). The study was conducted from August 2012 to June 2013, with typically one week of flights during each month (typically 3–5 flights each month) to characterize seasonality in mercury concentrations. The flight dates are listed in Table 2. Flights were conducted away from clouds in order to minimize potential scavenging of GOM and PBM into cloud drops and to avoid wetting the walls of the forward-facing inlet, with possible attendant losses. On the two occasions when the airplane flew through thin cloud layers during descent, GEM concentrations were not noticeably affected. GOM and PBM samples were conducted through these cloud layers; however, the duration of the flight through the thin cloud layers was only a few minutes, and the impacts appeared to be insignificant.

An advantage of using a twin-engine aircraft with outboard engines is that the forward fuselage area is free of exhaust contamination. Here, we extended the sampling inlets through the fuselage near the middle window on the starboard side. Sample air for the mercury speciation was brought into the onboard mercury system through a forward-facing 30 cm-long, 2 cm-diameter Teflon-coated aluminum tube protruding 15 cm into the free stream flow, with a volumetric flow rate of 20 L·m^{-1}. Due to its very short length (30 cm), the tube was left unheated. Sample air for the Tekran 2537, ozone and SO_2 instruments were obtained through a rear-facing Teflon tube protruding 8 cm into the free stream. A rear-facing inlet instead of a forward-facing inlet was used for the Tekran 2537 to minimize the effects of pressure changes due to speed changes during flight. Another advantage of using

different inlets for GEM and GOM/PBM was to have continuous GEM measurement during flight because the air flow was blocked intentionally by the valves shown in Figure 11 during some ascent/descent periods when all valves were closed. For the GOM/PBM sampling, a flow of 20 $L \cdot m^{-1}$ (*i.e.*, 2 × 10 $L \cdot m^{-1}$) was needed, so a forward-facing inlet was used, so the ram air could assist in meeting the flow requirements. Sample air for the CN counter was obtained through a rear-facing stainless steel tube (conductive, to avoid static charge buildup and loss of aerosols on the inlet. Tube lengths were minimized to avoid adsorptive loses. During the campaign, the Hg inlet tube was removed and periodically rinsed with DI water, which was subsequently analyzed for total mercury. The total mercury quantity in the rinsed water was found to be negligible. We concluded that oxidized Hg was not trapped by this short inlet tube.

Figure 11. Pictures showing the University of Tennessee Space Institute (UTSI) Navajo airplane, sample inlets through a window and the instrumentation inside the airplane. On top of the instrument rack is a box assembled with 8 denuders and 4 regenerable particle filters (RPFs) used to sample GOM and PBM, respectively.

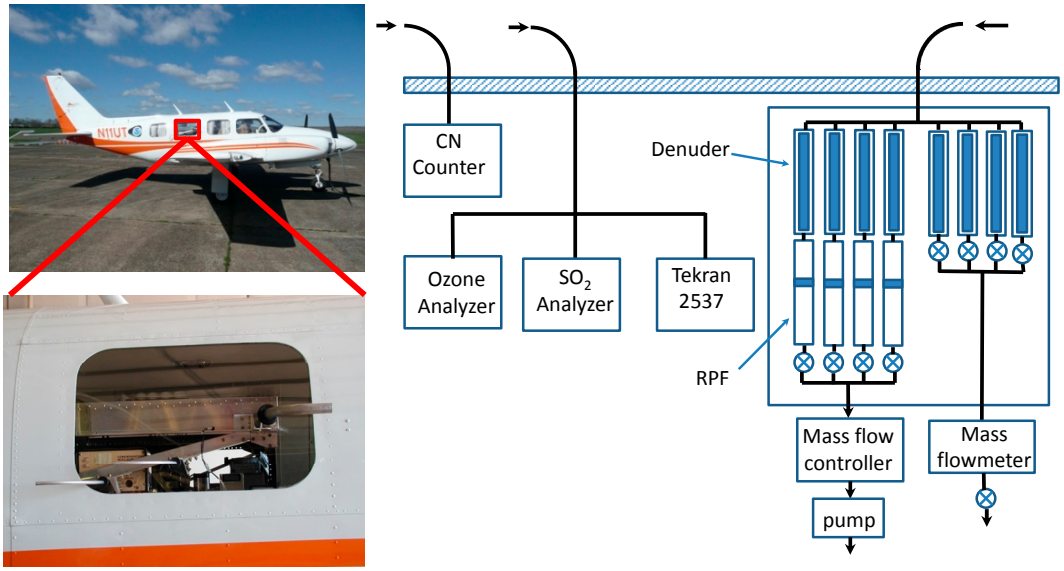

Table 2. Measurement flight months and dates.

Month	# of Flights	Dates
August, 2012	5	3,6,7,8 and 9 August
September, 2012	5	10,11,12,13 and 14 September
October, 2012	5	15,16,17,18 (day), 18 (night) October
November, 2012	4	13,14, 15 and 16 November
January, 2013	2	18 and 31 January
February, 2013	4	1,4,5 and 6 February
April, 2013	1	10 April
May, 2013	1	14 May
June, 2013	1	4 June
Total	28 Flights	

GEM was measured with an on-board Tekran ambient mercury vapor analyzer (Model 2537) based on cold vapor atomic fluorescence spectrophotometry (CVAFS) with a pressure controller on the cell vent to maintain a constant detection cell pressure (~780 Torr) at different altitudes. The instrument was operated with a sample cycle time of 2.5 min with a detection limit of about 0.1 ng m^3. Ozone was measured with a UV photometer constructed from components of a commercial detector (Model 49, Thermo Environmental Corporation, now Thermo Fisher Scientific, Waltham, MA, USA) mated to custom electronics for enhanced stability and response speed [26,27]. Sulfur dioxide was measured with a similarly modified pulsed fluorescence detector (Model 43s, Thermo Electron Corporation, Waltham, MA) optimized to minimize interferences posed by aromatic hydrocarbons and zeroed periodically with a carbonate-impregnated cellulose filter [28]. The number concentration of particles ranging in size from approximately 0.01 to 3 μm was measured with a TSI condensation nucleus counter (Model 3760). The particles are detected by condensing n-butanol on the particles, which allow them to grow to a size to be detected and counted by a laser-diode optical detector. All data were recorded at a 1-Hz frequency. The Tekran 2537 analyzer was calibrated using its internal Hg permeation source before each flight and periodically checked with an Hg calibrator (Tekran 2505) using manual injections. The O_3 detector was calibrated before and after the field campaign with a primary ozone standard. The SO_2 detector was calibrated weekly at concentrations ranging from 0–40 ppbv by dynamic dilution of a NIST-traceable compressed gas standard. No direct calibration for the CN counter is required, because particle pulses are well above the electronics noise level, and each pulse corresponds to exactly one particle. The detection limits were 1 ppbv for O_3 and 0.07 ppb for SO_2. The uncertainty for 1-min average concentrations is estimated to be ± (2 ppbv + 2% of reported concentration) for O_3 and ± (0.07 ppbv + 6% of reported concentration) for SO_2. GOM and PBM samples were collected on each flight using eight potassium chloride (KCl)-coated University Research Glassware (URG®) Corporation quartz denuders and four URG® regenerable particulate filters (RPFs), respectively, similar to those used in a Tekran Model 1130 Speciation Unit and a Model 1135 Particulate Mercury Unit, respectively. The volumetric sample flow rate through each denuder and RPF was maintained at 10 $L \cdot min^{-1}$ to ensure a constant residence time in the denuder. Each denuder pair/RPF assembly sampled air for about 30 min through a given altitude block (Figure 2). After each flight, denuder and RPF samples were immediately analyzed by heating them in a temperature-controlled tube furnace (set at 500 °C for denuder analysis and 800 °C for RPF analysis) and measuring the resulting, liberated mercury with a Tekran Model 2537 ambient mercury vapor analyzer. Concentrations of GOM and PBM were calculated based on the integrated elemental mercury driven off during heating and total sample volume corrected to standard conditions (*i.e.*, 0 °C and 1 atm). Field blank denuders (for GOM) and RPFs (for PBM) were deployed by installing them exactly the same as the sample denuders and RPFs, but with no air flow allowed. Both GOM and PBM blanks were very low and close to the detection limit of the Tekran 2537. During the normal sampling, denuders and RPFs were typically loaded with mercury amounts at least an order of magnitude greater than the blank levels. The average blank Hg level was about 0.8 pg for both GOM and PBM samples, and the detection limits were 2–3 $pg \cdot m^{-3}$. The GOM concentration differences between the replicate denuders collected for all samples at all altitudes averaged 13% with a standard deviation of 8.6%.

There are recent concerns that KCl denuders significantly underestimate GOM, particularly in the presence of high ozone [29,30]. This will be discussed further in the Conclusions section. Another bias

inherent in the collected dataset is a "sunny and clear" weather bias. Due to regulatory restrictions and safety concerns, the aircraft was not operated in rain, poor visibility or anytime there were significant cloud layers below about 7 km. Particularly in the summer months, this precluded many potential flight days.

3.2.2. Ground-Based Measurements

Measurements of GEM and GOM at a ground site at the airport were also made during the flight periods utilizing a Tekran 2537/1130 system (Toronto, ON, Canada) with the inlet ~1.3 m above the airport tarmac surface. The system was operated according to National Atmospheric Deposition Program Atmospheric's (NADP) Mercury Network (AMNet) protocol [31], except a shorter sample/analysis period (2.5 min) was used. The system was located next to a hangar where the aircraft parked. The system did not start to sample the ambient air until the aircraft was in the air, and there were few other airplanes around the hanger that were operated during ground-level sampling, so the risk of the sampling airplane exhaust was eliminated. A particulate mercury sample unit was not available for the ground-based measurements, due to resource constraints.

3.3. HYSPLIT Trajectory Model

Five-day back trajectory calculations were conducted for each high GOM and PBM event to establish the transport history of the associated air masses. The back trajectories were calculated using a PC version of the NOAA Hybrid Single-Particle Lagrangian Integrated Trajectory model (HYSPLIT, v4.9) [32] and the Eta Data Assimilation System (EDAS40) archive, having a horizontal resolution of 40 km × 40 km covering the continental United States, and 3-h time resolution. Trajectories were initialized from Tullahoma at 5 different altitudes (100 m, 1800 m, 3000 m, 4200 m and 5400 m) for the hours when the flights were conducted. These altitudes represent the surface and the typical middle altitudes of four altitude blocks where airborne GOM and PBM samples were collected.

4. Conclusions

Vertical profiling flights primarily for mercury species from the surface to ~6 km were conducted between August 2012 and June 2013, over central Tennessee, USA. Profiles were predominantly characterized by high spring/summer concentrations of gaseous oxidized mercury (GOM) up to 126 pg·m^{-3} (mean: 46 ± 30 pg·m^{-3} and range: ~6–126 pg·m^{-3}) and low fall/winter concentrations, ~10–20 pg·m^{-3}. The predominant vertical variation was low concentrations of GOM at the surface (1–5 pg·m^{-3}), peak concentrations at 2–4 km and decreasing concentrations extending to the highest altitude (6.1 km) at which measurements were conducted. The profiles of particulate bound mercury (PBM) showed some of the same general variations as observed for GOM, but were far less pronounced. The vertical and seasonal variation for gaseous elemental mercury (GEM) varied the least with concentrations ~1.4 ng·m^{-3} ± 10% for the entire vertical range and annual cycle.

Comparing our summer GOM profiles (Figure 5) to those airborne GOM measurements previously conducted by Swartzendruber *et al.* [1] (Supplemental Materials Figure S2) in July and August over Washington State, DC, USA, we see the same variation of low GOM concentrations in the boundary layer (<1–2 km), peak GOM concentrations in the 2–4 km range and decreasing GOM concentrations

above ~4 km. The technique used in Swartzendruber *et al.* [1] was based on the difference method (TGM-GEM), which they determined to be well correlated to the denuder method with a nearly consistent factor of two difference in concentrations (with KCl denuders showing less GOM concentrations). Over their five flights in July (one flight) and August (four flights), the maximum mean GOM concentrations at 2–4 km altitude were ~150 and 75 pg·m^{-3} for the difference and denuder methods, respectively [1]. This latter concentration is remarkably close to our (denuder) mean August (four flights) GOM concentration of 73 pg·m^{-3} at 2–4 km.

For future measurement of oxidized mercury Gustin *et al.* [30] recommends total pyrolyzer methods over the use of KCl-coated denuders. We could not take the suggestions from this 2013 publication, because our measurement began in 2012. There are current concerns that the KCl denuders used in this study may significantly under-collect GOM, especially in the presence of enhanced ozone [29,30]. GOM collections also suffer from a lack of calibration standards [33]. However, there are challenges with both the denuder and total pyrolyzer techniques. Despite these concerns, KCl denuders are currently utilized by the Tekran model 1130 and by the National Atmospheric Deposition Program Atmospheric Mercury Network (AMNet). In light of the above, the GOM concentrations reported here may be biased low, particularly in the summer months, when ozone is elevated. We feel that this potential bias does not significantly affect our main findings regarding the vertical profiles of the Hg species profiles and their seasonality. Swartzendruber *et al.* [1] utilized KCl denuders and a pyrolyzer unit concurrently on their aircraft and determined a roughly consistent factor of ~2 difference in concentrations, with KCl denuders showing less GOM. As presented, our GOM results match well with Swartzendruber *et al.*'s [1] KCl denuder GOM results. If we doubled our oxidized mercury reported results, then these revised results would closely match the pyrolyzer (TGM-GEM) results of Swartzendruber *et al.* [1]. Results from CTM-Hg, GEOS-Chem and GRAHM are consistent with our observations up to 4 km, predicting low GOM concentrations in the near surface air with enhancements beginning above the boundary layer and concentrations in the range of ~30 to 120 pg·m^{-3} at an altitude of 3 km [7]. However, none of these models predict our and Swartzendruber's *et al.*'s [1] observed decrease in GOM concentrations above 4 km. All of these models show a positive (increasing) GOM concentration gradient at 4–5 km. Here, we find these modeled results of the increased oxidation rate above ~4 km to be inconsistent with our "summer" GOM profiles and the previous mean summer GOM concentration profile of Swartzendruber *et al.* [1]. It is possible that these current models overestimate the GEM oxidation in the 4–6 km range.

Our GOM concentration profiles are consistent with other indirect measurements of free-tropospheric GOM. Greatly elevated GOM concentrations in the free troposphere relative to normal ground-based measurements have been reported from mountain peak measurement sites under special conditions where free tropospheric air has been rapidly mixed downward [4,5].

Our measurements over Tullahoma showed generally that GOM concentrations peaked at an altitude of ~2–4 km, where it was 10–30-times higher than GOM concentrations in the near surface air. GOM and PBM concentrations showed their lowest concentrations at the lowest altitudes where boundary layer entrainment leads to surface deposition. Ground-based GOM concentration was not significantly correlated (r^2 = 0.13) to the maximum GOM concentration in the profile, making assessment of the GOM column difficult from just ground-based measurements. GOM concentrations showed a strong seasonality with "winter" minima in November to February and "summer" maxima in

April to August. PBM concentration, similar to GOM concentration, showed "winter" minima in January and February.

We find that some current models (e.g., CTM-Hg, GEOS-Chem and GRAHM) [11] appear to "miss" the summer decrease in GOM concentration above 4 km observed here and by Swartzendruber *et al.* [1]. We suggest that possibly these current models overestimate the GEM oxidation rate in the 4–6 km range.

Here, we have presented for the first time a set of speciated mercury profiles at a single location over the course of a year. Users of these data are cautioned that these measurements are biased towards "clear sunny days" due to safety concerns of flying in the rain, poor visibility or cloud layers below 7 km.

Acknowledgments

This study was funded by the National Oceanic and Atmospheric Administration (NOAA) (Project #: NA09OAR4600198 and NA10OAR4600209). We thank the University of Tennessee Space Institute flight crew, Devon Simmons, Gregory Heatherly, Samuel Williams and Jacob Bowman, for their dedicated work to make the airborne measurements successful. Support for this research was also partially provided by the Cooperative Institute for Climate and Satellites agreement funded by NOAA's Office of Oceanic and Atmospheric Research under a NOAA Cooperative Agreement.

Author Contributions

Steve Brooks and Xinrong Ren wrote the manuscript and performed much of the data analysis. Steve Brooks, Xinrong Ren, Winston T. Luke, Paul Kelley, Mark Cohen, Richard Artz, Anthony Hynes, William Landing and Borja Martos were involved in the planning, preparation and data collection in the field deployment. Mark Cohen helped with HYSPLIT trajectory simulations and provided scientific insight and editing.

Conflicts of Interest

The authors declare no conflict of interest.

References

1. Swartzendruber, P.C.; Jaffe, D.A.; Finley, B. Development and first results of an aircraft-based, high time resolution technique for gaseous elemental and reactive (oxidized) gaseous mercury. *Environ. Sci. Technol.* **2009**, *43*, 7484–7489.
2. Murphy, D.M.; Hudson, P.K.; Thomson, D.S.; Sheridan, P.J.; Wilson, J.C. Observations of mercury-containing aerosols. *Environ. Sci. Technol.* **2006**, *40*, 3163–3167.
3. Lyman, S.N.; Jaffe, D.A. Formation and fate of oxidized mercury in the upper troposphere and lower stratosphere. *Nat. Geosci.* **2012**, *5*, 114–117.
4. Fain, X.; Obrist, D.; Hallar, A.G.; Mccubbin, I.; Rahn, T. High levels of reactive gaseous mercury observed at a high elevation research laboratory in the Rocky Mountains. *Atmos. Chem. Phys.* **2009**, *9*, 8049–8060.

5. Swartzendruber, P.C.; Jaffe, D.A.; Prestbo, E.M.; Weiss-Penzias, P.; Selin, N.E.; Park, R.; Jacob, D.J.; Strode, S.; Jaegle, L. Observations of reactive gaseous mercury in the free troposphere at the Mount Bachelor Observatory. *J. Geophys. Res.: Atmos.* **2006**, doi:10.1029/2006JD007415.
6. Gay, D.A.; Schmeltz, D.; Prestbo, E.; Olson, M.; Sharac, T.; Tordon, R. The atmospheric mercury network: Measurement and initial examination of an ongoing atmospheric mercury record across North America. *Atmos. Chem. Phys.* **2013**, *13*, 11339–11349.
7. Bullock, O.R.; Atkinson, D.; Braverman, T.; Civerolo, K.; Dastoor, A.; Davignon, D.; Ku, J.Y.; Lohman, K.; Myers, T.C.; Park, R.J.; *et al.* The North American Mercury Model Intercomparison Study (NAMMIS): Study description and model-to-model comparisons. *J. Geophys. Res.: Atmos.* **2008**, doi:10.1029/2008JD009803.
8. Seigneur, C.; Karamchandani, P.; Lohman, K.; Vijayaraghavan, K.; Shia, R.L. Multiscale modeling of the atmospheric fate and transport of mercury. *J. Geophys. Res.: Atmos.* **2001**, *106*, 27795–27809.
9. Selin, N.E.; Jacob, D.J.; Yantosca, R.M.; Strode, S.; Jaegle, L.; Sunderland, E.M. Global 3-D land-ocean-atmosphere model for mercury: Present-day *versus* preindustrial cycles and anthropogenic enrichment factors for deposition. *Glob. Biogeochem. Cycles* **2008**, doi:10.1029/2007GB003040.
10. Dastoor, A.P.; Larocque, Y. Global circulation of atmospheric mercury: A modelling study. *Atmos. Environ.* **2004**, *38*, 147–161.
11. Holmes, C.D.; Jacob, D.J.; Corbitt, E.S.; Mao, J.; Yang, X.; Talbot, R.; Slemr, F. Global atmospheric model for mercury including oxidation by bromine atoms. *Atmos. Chem. Phys.* **2010**, *10*, 12037–12057.
12. Nair, U.S.; Wu, Y.; Justin, W.; Jansen, J.; Edgerton, E.S. Diurnal and seasonal variation of mercury species at coastal-suburban, urban, and rural sites in the southeastern United States. *Atmos. Environ.* **2012**, *47*, 499–508.
13. Holmes, C.D.; Jacob, D.J.; Yang, X. Global lifetime of elemental mercury against oxidation by atomic bromine in the free troposphere. *Geophys. Res. Lett.* **2006**, doi:10.1029/2006GL027176.
14. Lin, C.J.; Pongprueksa, P.; Lindberg, S.E.; Pehkonen, S.O.; Byun, D.; Jang, C. Scientific uncertainties in atmospheric mercury models I: Model science evaluation. *Atmos. Environ.* **2006**, *40*, 2911–2928.
15. Sommar, J.; Gardfeldt, K.; Stromberg, D.; Feng, X.B. A kinetic study of the gas-phase reaction between the hydroxyl radical and atomic mercury. *Atmos. Environ.* **2001**, *35*, 3049–3054.
16. Pal, B.; Ariya, P.A. Gas-phase HO center dot-Initiated reactions of elemental mercury: Kinetics, product studies, and atmospheric implications. *Environ. Sci. Technol.* **2004**, *38*, 5555–5566.
17. Tossell, J.A. Calculation of the energetics for oxidation of gas-phase elemental Hg by Br and BrO. *J. Phys. Chem. A* **2003**, *107*, 7804–7808.
18. Goodsite, M.E.; Plane, J.M.C.; Skov, H. A theoretical study of the oxidation of Hg^0 to $HgBr_2$ in the troposphere. *Environ. Sci. Technol.* **2004**, *38*, 1772–1776.
19. Goodsite, M.E.; Plane, J.M.C.; Skov, H. Correction to a theoretical study of the oxidation of Hg^0 to $HgBr_2$ in the troposphere. *Environ. Sci. Technol.* **2012**, *46*, 5262–5262.
20. Calvert, J.G.; Lindberg, S.E. Mechanisms of mercury removal by O-3 and OH in the atmosphere. *Atmos. Environ.* **2005**, *39*, 3355–3367.

21. Hynes, A.J.; Donohoue, D.L.; Goodsite, M.E.; Hedgecock, I.M. Our current understanding of major chemical and physical processes affecting mercury dynamics in the atmosphere and at the air-water/terrestrial interfaces. In *Mercury Fate and Transport in the Global Atmosphere: Emissions, Measurements and Models*; Pirrone, N., Mason, R.P., Eds.; Springer: Berlin, Germany, 2009; pp. 427–457.
22. Seigneur, C.; Lohman, K. Effect of bromine chemistry on the atmospheric mercury cycle. *J. Geophys. Res.: Atmos.* **2008**, doi:10.1029/2008JD010262.
23. Dastoor, A.P.; Davignon, D.; Theys, N.; Van Roozendael, M.; Steffen, A.; Ariya, P.A. Modeling dynamic exchange of gaseous elemental mercury at polar sunrise. *Environ. Sci. Technol.* **2008**, *42*, 5183–5188.
24. Fishman, J.; Crutzen, P. *The Distribution of the Hydroxyl Radical in the Troposphere*; Department of Atmospheric Science. Colorado State University: Fort Collins, CO, USA, 1978.
25. Berresheim, H.; Plass-Dulmer, C.; Elste, T.; Mihalopoulos, N.; Rohrer, F. OH in the coastal boundary layer of Crete during MINOS: Measurements and relationship with ozone photolysis. *Atmos. Chem. Phys.* **2003**, *3*, 639–649.
26. Luke, W.T.; Arnold, J.R.; Watson, T.B.; Dasgupta, P.K.; Li, J.Z.; Kronmiller, K.; Hartsell, B.E.; Tamanini, T.; Lopez, C.; King, C. The NOAA Twin Otter and its role in BRACE: A comparison of aircraft and surface trace gas measurements. *Atmos. Environ.* **2007**, *41*, 4190–4209.
27. Luke, W.T.; Kelley, P.; Lefer, B.L.; Flynn, J.; Rappengluck, B.; Leuchner, M.; Dibb, J.E.; Ziemba, L.D.; Anderson, C.H.; Buhr, M. Measurements of primary trace gases and NOy composition in Houston, Texas. *Atmos. Environ.* **2010**, *44*, 4068–4080.
28. Luke, W.T. Evaluation of a commercial pulsed fluorescence detector for the measurement of low-level SO_2 concentrations during the gas-phase sulfur intercomparison experiment. *J. Geophys. Res.: Atmos.* **1997**, *102*, 16255–16265.
29. Lyman, S.N.; Jaffe, D.A.; Gustin, M.S. Release of mercury halides from KCl denuders in the presence of ozone. *Atmos. Chem. Phys.* **2010**, *10*, 8197–8204.
30. Gustin, M.S.; Huang, J.Y.; Miller, M.B.; Peterson, C.; Jaffe, D.A.; Ambrose, J.; Finley, B.D.; Lyman, S.N.; Call, K.; Talbot, R.; *et al.* Do we understand what the mercury speciation instruments are actually measuring? Results of RAMIX. *Environ. Sci. Technol.* **2013**, *47*, 7295–7306.
31. Ren, X.; Luke, W.T.; Kelley, P.; Cohen, M.; Ngan, F.; Artz, R.; Walker, J.; Brooks, S.; Moore, C.; Swartzendruber, P.; *et al.* Mercury speciation at a coastal site in the northern Gulf of Mexico: Results from the Grand Bay intensive studies in summer 2010 and spring 2011. *Atmosphere* **2014**, *5*, 230–251.
32. Draxler, R.R.; Rolph, G.D. *HYSPLIT (HYbrid Single-Particle Lagrangian Integrated Trajectory) Model*; NOAA Air Resources Laboratory: College Park, MD, USA, 2014.
33. Steffen, A.; Scherz, T.; Olson, M.; Gay, D.; Blanchard, P. A comparison of data quality control protocols for atmospheric mercury speciation measurements. *J. Environ. Monit.* **2012**, *14*, 752–765.